Impact of Phase Noise on Mutual Interference of FMCW and PMCW Automotive Radars

H.C. Yildirim*, M. Bauduin†, A. Bourdoux† and F. Horlin*
*Université Libre de Bruxelles (ULB) - †Interuniversity Micro-Electronics Center (Imec)

Email: *hasan.can.yildirim@vub.be, {marc.bauduin,andre.bourdoux}@imec.be, fhorlin@ulb.ac.be*

***Abstract*—During the last decade, the demand of smart sensors for advanced driving assistance systems (ADAS) has increased in order to keep the road safety at a sufficient level. For ADAS, one of the most widely considered sensors are radars. In the next few years, it is expected that each new car model will be equipped with many radars providing a 360°view of the scene. Due to the significant increase of number of radars in heavy traffic conditions, it is expected that the interferences among those radars will significantly reduce their reliability. Unfortunately, analog front-end imperfections such as phase noise are known to aggravate the interference problem. Since there is no standardisation of the radar waveforms, the radar designers are free to choose the best waveforms to minimise the impact of the interferences on the radar performance. Our aim is to compare the robustness of frequency-modulated continuous wave (FMCW) and phase-modulated continuous wave (PMCW) waveforms to mutual interference when the radars are subject to phase noise. A mathematical model of the radar is built to formalise the problem and numerical results are provided in order to assess the degradations on range-Doppler Maps.**

***Index Terms*—Automotive radar, ADAS, mutual interference, FMCW, PMCW, phase noise**

I. Introduction

The interference between automotive radars, densely deployed on the road, may significantly reduce the radar performance. The MOSARIM project, funded by EU [1], aimed to identify the main consequences caused by mutual interference (MI) on the range-Doppler map (RDM) generated at the output of the radar processing. The final deliverable of this project showed that MI plays an important role in radars for ADAS applications.

The impact of MI between FMCW and PMCW radars is studied in [2], by also considering carrier frequency offset between the interfering and victim radars. It is shown by simulations that cross waveform interferences (FMCW-to-PMCW or vice-versa) mainly increases the noise floor, while the interferences between radars using the same waveform (FMCW-to-FMCW or PMCW-to-PMCW) yield various degradations on RDMs. In [3], a closed-form expression of the MI is provided and validated by simulations assuming that the FMCW or PMCW waveform durations can be varying. In [4], MI between triangular slow time FMCW chirps are further considered. On the other hand, papers such as [5] investigate how MI mitigation techniques could be implemented.

In the presence of MI, the analog front-end non-idealities play an important role, but their impact is not well addressed in the literature. In [6], the impact of phase noise (PN) is analysed for FMCW radars without considering interference among radars. However, the attenuation of PN at short distance (also known as correlated PN) does not apply in MI scenario since the interfering PN is uncorrelated, as studied in [7]. Therefore, it is expected that PN will have higher impact when MI scenarios are considered. In this work, we study MI of separate FMCW and PMCW automotive radars subject to PN. We provide closed-form expressions to correctly understand the impact of the MI. Numerical results further assess the impact of MI on the output RDMs.

The structure of this paper is as follows: In Section II, both waveform models are introduced. In Section III, the mathematical models are extended for interference scenarios with PN. In Section IV, numerical results are provided. Finally, in Section V, the conclusion is drawn.

II. FMCW and PMCW Radar Models

A brief description of FMCW and PMCW radars is given in this section. For more information on both radar systems, the reader is referred to [8].

A. FMCW

An FMCW waveform is characterized by its bandwidth B and sweep duration T, where its slope can be defined as $\alpha = \frac{B}{T}$. The complex baseband equivalent of FMCW waveform for one chirp can be defined as,

$$s_{FM}(t) = \exp(j\pi\alpha t^2), \;\; 0 \leq t < T \tag{1}$$

and the chirp is repeated periodically: $s_{FM}(t) = s_{FM}(t+T)$. Then the received waveform, for a target at distance R, can be written as,

$$r_{FM}(t) = A_2 s_{FM}(t-\tau)\exp(j2\pi f_d t) \tag{2}$$

where A_2, $\tau = \frac{2R}{c}$ and $f_d = \frac{\pm 2v}{\lambda}$ represents the attenuation, propagation delay and Doppler frequency under two-way propagation; R, c, v and λ represents the initial distance, speed of light, speed of the target and the carrier wavelength, respectively. Since the direction of the movement affects the sign of the Doppler shift, '$\pm$' sign is used. At the receiver, the received signal is multiplied by the complex conjugate of the transmitted signal, which yields the de-chirped signal,

$$r_{dec}(t) = A_2 \exp(-j2\pi(\alpha\tau - f_d)t)\exp(-j\pi(\alpha\tau^2)) \tag{3}$$

Here, the first exponential contains the interesting information for range and speed estimation. The second exponential

contains a constant phase, and since it is much smaller than time varying terms, it can be ignored. After sampling at frequency f_s ($t = m/f_s$), the de-chirping process is repeated for N range profiles, and the results are stacked on a matrix,

$$r[m,n] = A_2 \exp(-j2\pi(\alpha\tau - f_d)\frac{m}{f_s} + j2\pi f_d nT) \quad (4)$$

where $0 \leq n < N$, and $0 \leq m < M-1$ where m is the samples of a dechirped signal. Here, the dimension m (called fast-time processing yielding to range dimension) contains the propagation delay information affected by the Doppler. The dimension n (called slow-time processing yielding to speed dimension) can be used to identify moving targets. By computing the FFT on both dimensions of (4), RDMs can be generated. Because of the FMCW ambiguity function, the range and Doppler effect are coupled: they both impact the range estimation.

B. PMCW

A PMCW waveform is characterized by the system bandwidth and the modulating sequence. In this paper, we only consider bi-phase modulations such that the two phases are $\{0, \pi\}$ for the sequence elements of $\{-1, 1\}$. The PMCW waveform can be written as,

$$s_{PM}(t) = \sum_{k=0}^{K-1} I_k g(t - kT_c), \quad 0 \leq t < T \quad (5)$$

where I_k is the sequence element. $g(t)$ is a unit amplitude pulse shaping filter on the time interval $[0, T_c)$, where $T_c = 1/B$ is the chip duration and K is the sequence length. The total duration of one PMCW waveform is $T = KT_c$. Also, transmitted PMCW waveform is considered to be periodic, such that $s_{PM}(t) = s_{PM}(t+T)$. We can define the received PMCW waveform, for a target at distance R, as follows,

$$r_{PM}(t) = A_2 s_{PM}(t - \tau) \exp(j2\pi f_d t) \quad (6)$$

After sampling the received signal, and computing the auto-correlation between (5) and (6),

$$r[m,n] = \sum_{k=0}^{K-1} (I_k I_{k-\tau_d+m}) \exp(j2\pi f_d(nT + (m+k)T_c)) \quad (7)$$

can be derived, where $\tau_d = \left\lfloor \frac{2R}{cT_c} \right\rfloor$ represents the shift on the sequence due to the two-way propagation delay. Similar to (4), (7) contains the range information along m dimension. The Almost-Perfect-Autocorrelation-Sequences (APS) proposed in [9], provides a range profile with zero-correlation-zones (ZCZ). The second dimension of (7) contains the phase changes of each range bin caused by the Doppler shift (nT). Since a moving target changes the phases of the chips in a sequence as well ($(m+k)T_c$), the received sequence will not be a pure binary sequence. This creates small sidelobes along the range profile. It is clear that, for PMCW radars, the range-Doppler estimations are not coupled.

III. Mutual Interference under Phase Noise

In real-life radar implementations, the oscillator, which is used to generate the carrier frequency, is not completely stable. Therefore, the generated frequency is corrupted by a filtered noise. The oscillator output can be modelled as follows,

$$s_{LO,PN}(t) = \exp(j2\pi f_c t) \exp(j\phi(t)) \quad (8)$$

where $\phi(t)$ and f_c represent the PN and the carrier frequency, respectively. Since $s_{LO,PN}(t)$ is used for shifting the baseband signal to the carrier frequency, the generated radio frequency (RF) signal will suffer from some additional noise components. Since separate oscillators are used for the interferer and victim, PN carried by the interfering signal, wears additional uncorrelated noise components at the victim receiver [7]. In Figure 1, we provide the power spectral density (PSD) of the PN that is considered in this work. The reader is referred

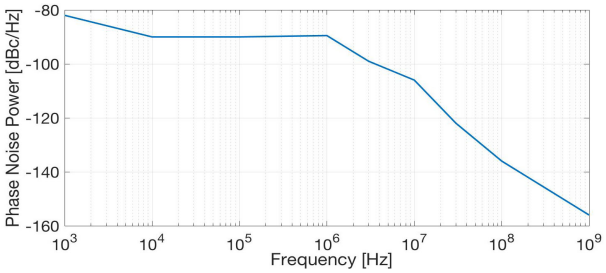

Fig. 1: PSD of measured PN from IMEC's PMCW radar [10]

to [11] for a detailed description of the phase noise. It is also important to mention that PN is a multiplicative process, meaning that improving the SNR does not have any effect on it. For the simplicity of notation, the parameters of interferer and victim will be identified by using 'i' and 'v' as subscripts, respectively.

A. FMCW

The received interference FMCW waveform with PN can be written as,

$$r_{FM,i}(t) = A_1 \exp(j\pi(\alpha_i(t-\tau_i)^2 + 2f_{d,i}t) + j\phi(t-\tau_i)) \quad (9)$$

where $\alpha_i = \frac{B_i}{T_{s,i}}$ is the chirp slope of the interfering signal. Here, attenuation A_1, propagation delay $\tau_i = \frac{R_i}{c}$ and Doppler frequency $f_{d,i} = \frac{v_i}{c}$ are defined for one-way propagation. The de-chirped interfering signal can be written as,

$$\begin{aligned} r_{dec,i}(t) &= A_1 \exp(-j\pi(\alpha_i - \alpha_v)t^2) \\ &\cdot \exp(-j2\pi(\alpha_i\tau_i - f_{d,i})t + j\phi(t-\tau_i)) \end{aligned} \quad (10)$$

where small varying phase terms are ignored. By following the radar processing principles from subsection II-A,

$$\begin{aligned} r_i[m,n] &= A_1 \exp(-j\pi(\alpha_i - \alpha_v)(m/f_s)^2) \\ &\cdot \exp(-j2\pi(\alpha_i\tau_i + f_{d,i})m/f_s) \\ &\cdot \exp(j2\pi f_{d,i} n T_{s,v} + j\phi(m/f_s - \tau_i)) \end{aligned} \quad (11)$$

can be written. In (11), the first exponential is an additional effect due to the interference. If the bandwidth and chirp duration are equal for interferer and victim, this term will cancel out. Since the radar receiver is designed by assuming that waveforms propagate two-way, the second and third exponentials will create a ghost target with a strong peak at the half of the interferer true distance and speed. The PN term in the last exponential, will affect the whole range profile, i.e.

each range bin, m, will contain samples of PN. In case of a mismatch in the signal parameters of the interferer and victim, the first exponential will act like another FMCW modulation. Therefore, additional degradations, also known as ridges, will be observed, which are well-explained in [4]. In such a case, the ridges will cause the PN to spread in the range dimension.

However, in FMCW radar systems the maximum range is limited by the cut-off frequency of the lowpass filter (LPF, located before the analog-to-digital converter). If signal parameters are equal, and if the frequency of the ghost-target exceeds the cut-off frequency of LPF, the ghost-target will be filtered out. As a consequence, no additional degradations will appear on RDM.

B. PMCW

We can write the received interfering PMCW waveform as follows,

$$\begin{aligned} r_{PM,i}(t) &= A_1 \sum_{l=0}^{L-1} I_{l,i} g(t - lT_{c,i} - \tau_i) \\ &\cdot \exp(j2\pi f_{d,i} t + j\phi(t - \tau_i)) \end{aligned} \quad (12)$$

where $I_{l,i}$ is the code sequence of the interfering radar, with code length of L. Similarly, the radar matrix elements can be written as,

$$\begin{aligned} r_i[m,n] &= \sum_{k=0}^{K-1} (I_{k,v} I_{k,i-\tau_{d_i}+m}) \\ &\cdot \exp(j2\pi f_{d,i}(nT + (m+k)T_{c,v})) \\ &\cdot \exp(j\phi((nT + (m+k)T_{c,v}) - \tau_i)) \end{aligned} \quad (13)$$

where $\tau_{d_i} = \left\lfloor \frac{R_i}{cT_{c,v}} \right\rceil$ is the shift of the sequence due to one-way propagation delay. In (13), there are two main possibilities. First, if the parameters of both interfering and victim radar are equal, it only leads to a ghost target. The exponential term with PN causes degradations on range and Doppler dimensions. For the range dimension, PMCW waveform relies on auto-correlation properties of the sequences. Therefore, when PN is present, ripples over range profile may appear due to small random shifts on the zero-crossings of the received interfering sequence. Doppler dimension, on the other hand, will contain the phase noise samples from the interferer. Therefore, when the FFT is computed for Doppler estimation on the second dimension of (13), additional degradations may appear. Second, if the code sequence and/or the bandwidth of the interfering signal are/is different, the auto-correlation will become a cross-correlation with a modified sequence. Since APS are not designed for ideal cross-correlations, the RDM will contain ridges. Therefore, the energy of the PN will spread through range dimension.

IV. Numerical Results

The equations (11) and (13) can be particularised for different FMCW or PMCW waveform parameters. In [2], it is shown that a complete mismatch between the victim and interferer waveform parameters yields an increased noise floor in the RDM. In [3], it is further shown that a waveform duration mismatch yields multiple ridges. In order to clearly observe the impact of the PN, we focus on two representative cases in this work: the waveforms are in complete match; there is only a bandwidth mismatch.

We define a radar scene where three targets are present:

- Two cars (12m/s, 20m, 10dBsm) and (-15m/s, 15m, 10dBsm); The first car is equipped with the interfering radar.
- A target such as a bike: (-1m/s, 5m, 2dBsm)

For FMCW radars, only positive slopes are considered. The APS sequences are used for modulating the PMCW waveforms. The waveform parameters of the victim are fixed to the values given in Table I. These parameters provide 0.15m range and 0.6m/s speed resolutions. The parameters of the interferer will vary. Transmit powers, antenna gains, system losses and carrier frequencies of both victim and interferer are 10dBm, 10dBi, 3dB and 79GHz, respectively. The noise figure of the victim receiver is 6dB. Finally, the noise is normalised to 0dB in RDM plots. In order to suppress the sidelobes inherent to the waveforms, a Blackman window is applied to both range and Doppler dimensions for FMCW, and only to Doppler dimension for PMCW.

Radar	Waveform	Parameters
Victim	FMCW	$V_{fm}(B = 1GHz, T = 20\mu s)$
	PMCW	$V_{pm}(B = 1GHz, K = 504)$
Interferer	FMCW	$I_{fm}(B, T)$
	PMCW	$I_{pm}(B, K)$

TABLE I: Waveform parameters for simulation scenarios.

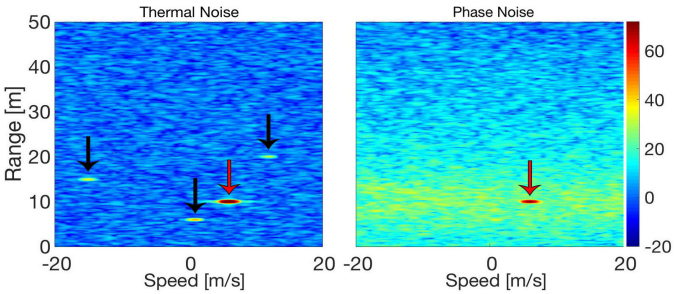

Fig. 2: FMCW: $I_{fm}(1GHz, 20\mu s)$

In Figure 2, we provide the RDM at the output of the FMCW radar when the interferer is fully matched to the victim. If there is only thermal noise (TN), we see the three targets, indicated by black arrows. At the half of interferer true distance and speed, a ghost target appears as a much stronger peak, indicated by the red arrow. When the PN is added to the simulations, we can see that there is a mask on top of the TN centred on the ghost target. This effect can be explained by (11). After de-chirping, the spectral energy is focused on a specific frequency bin, m_i. However, all the other values of m contain residuals from the PN. The noise level increases by about 40 dB around the target in such a way that all three actual targets are hidden by the PN.

In Figure 3, we provide the RDM at the output of the PMCW radar when the interferer is fully matched to the victim. When there is only TN, the true targets and the ghost target appear as expected. When PN is added, an additional

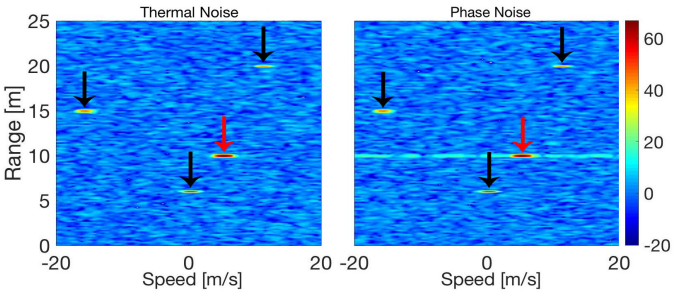

Fig. 3: PMCW: $I_{pm}(1GHz, 504)$. Maximum range is limited to 25 meters for the plot.

ridge can be observed at a level equal to 12dB higher than the noise floor. Since PMCW does not suffer from range-Doppler coupling, and thanks to the zero range sidelobes of the APS in the region of interest, the ridge is located at a particular range bin and additional noise components spread only through the Doppler dimension. Therefore, only the targets located at the same range with the ghost target may be hidden by the PN. For both FMCW and PMCW, the magnitude of the ghost target also depends on the distance of the interferer. For an interferer at closer distance, PN mask will appear at a high magnitude (and vice-versa for interferers at further distance). Therefore, when fully synchronous cases are considered, removing the ghost target at detection level will not be sufficient.

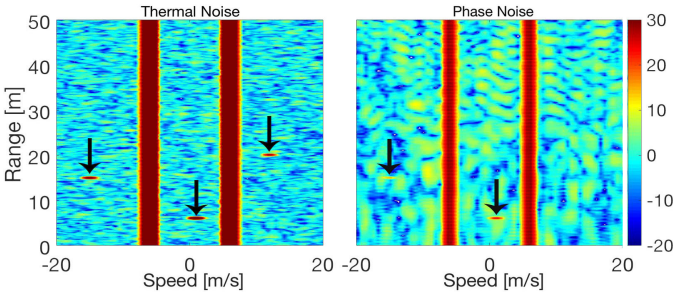

Fig. 4: FMCW: $I_{fm}(0.45GHz, 20\mu s)$

In Figure 4, we provide the RDM at the output of the FMCW radar when there is a bandwidth mismatch between the victim and the interferer. Since the waveform parameters are not the same, the response of the radar to the interferer is not anymore focused on a specific range bin and it spreads over all range bins (ridges through the range profile). The ridges also spread to the opposite sign of the speed since two chirps with different slopes yield both negative and positive frequencies after de-chirping. This effect is explained in [4]. Since there is no focused energy on a specific range bin, additional noise also spreads and causes an increase of the noise floor to a level of about 10 dB. Therefore, instead of observing the hill-like shape of PN, a mask with flat energy appears everywhere in the RDM. In such a case, one of the targets is hidden under the noise, while the others are still visible.

Finally, in Figure 4, we provide the RDM at the output of the PMCW radar when there is a bandwidth mismatch between the victim and the interferer. In the presence of TN, we observe only one ridge and it is located at the half of the speed of the interferer. When PN is added, we observe that the power of the

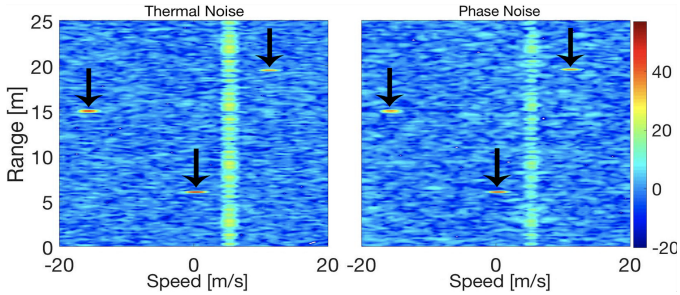

Fig. 5: PMCW: $I_{pm}(0.45GHz, 504)$

ridge is reduced. This effect can be explained by (13). The PN spreads the power of the interfering signal to several range and Doppler bins. Since the total power of the interfering signal at the receiver should remain constant, the spreading effect causes an attenuation on the ridge.

V. Conclusion

The impact of mutual interference on FMCW and PMCW radars has been analysed when the analog front-ends suffer from phase noise. A closed-form expression of the MI is provided and numerically assessed by simulations. PMCW radars show a better robustness against PN than FMCW radars. The robust behaviour is observed when the parameters of the victim and interferer are identical or when there is a bandwidth mismatch. Our analysis shows that mutual interference strongly depends on the hardware non-idealities.

References

[1] M.e.a. Kunert, "Mosarim - project final report," 2012.
[2] A. Bourdoux, K. Parashar, and M. Bauduin, "Phenomenology of Mutual Inferference of FMCW and PMCW Automotive Radars," in *RadarConf*.
[3] H-P Beise, T. Stifter, and U. Schröder, "Virtual Interference Study for FMCW and PMCW Radar," in *GeMIC, 2018*.
[4] M. Goppelt, H.-L. Blocher, and W. Menzel, "Automotive Radar Investigation of Mutual Interference Mechanisms," 2010.
[5] J. Bechter, F. Ross, M. Rahman, and C. Waldschimidt, "Automotive Radar Interference Mitigation using Sparse Sampling Approach," in *EURAD, 2017*.
[6] K. Siddiq, R.J. Watson, P. Avery, R. Poulton, and B. Dakin-Norris, "Phase noise analysis in FMCW radar systems," in *EuRAD, 2015*.
[7] M.C. Budge and M.P. Burt, "Range Correlation Effects in Radars," 1993.
[8] Mark A. Richards, James A. Scheer, and William A. Holm, *Principles of Modern Radar: Basic Principles*, Scitech Publishing, 2010.
[9] W. Van Thillo, P. Gioffre, V. Giannini, D. Guermandi, S. Brebels, and A. Bourdoux, "Almost Perfect Auto-correlation Sequences for Binary Phase-modulated Continuous Wave Radar," in *EuRAD, 2013*.
[10] A. Bourdoux, V. Giannini, D. Guermandi, S. Brebels, and W. Van Thillo, "Impact of Phase Noise on High Resolution Phase-coded Continuous mm-wave Radars," in *GSMM 2013*.
[11] Stanley J. Goldman, *Phase Noise Analysis in Radar Systems Using Personal Computers*, Wiley-Interscience, 1989.